NSWC/WOL/TR 75-49

NSWC/WOL/TR 75-49

AD A013219

NSWC

TECHNICAL REPORT

WHITE OAK LABORATORY

VERTICAL WATER ENTRY OF SPHERES

BY
John L. Baldwin
Howard K. Steves

7 MAY 1975

NAVAL SURFACE WEAPONS CENTER
WHITE OAK LABORATORY
SILVER SPRING, MARYLAND 20910

• Approved for public release; distribution unlimited

DDC
RECEIVED
AUG 11 1975
A

NAVAL SURFACE WEAPONS CENTER
WHITE OAK, SILVER SPRING, MARYLAND 20910

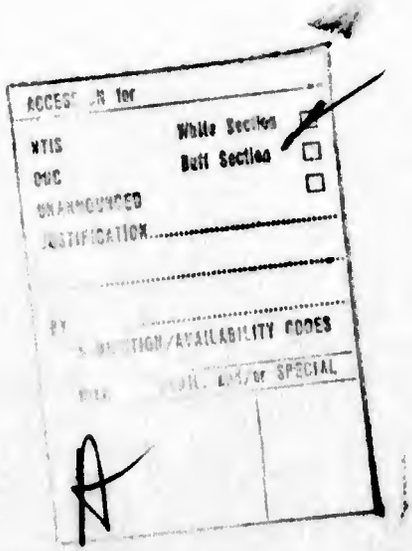
ACCESSION for
NTIS
DDC
UNANNOUNCED
JUSTIFICATION
White Section
Buff Section
BY
DISTRIBUTION/AVAILABILITY CODES
DIST. AVAIL. and/or SPECIAL
A

UNCLASSIFIED

SECURITY CLASSIFICATION OF THIS PAGE (When Data Entered)

REPORT DOCUMENTATION PAGE

READ INSTRUCTIONS BEFORE COMPLETING FORM

1. REPORT NUMBER: NSWC/WOL/TR-75-49
2. GOVT ACCESSION NO.:
3. RECIPIENT'S CATALOG NUMBER:
4. TITLE (and Subtitle): Vertical Water Entry of Spheres.
5. TYPE OF REPORT & PERIOD COVERED: Technical rept. Interim
6. PERFORMING ORG. REPORT NUMBER:
7. AUTHOR(s): John L. Baldwin, Howard K. Steves
8. CONTRACT OR GRANT NUMBER(s):
9. PERFORMING ORGANIZATION NAME AND ADDRESS: Naval Surface Weapons Center, White Oak, Silver Spring, Maryland 20910
10. PROGRAM ELEMENT, PROJECT, TASK AREA & WORK UNIT NUMBERS: ORD-35B-001/UR109-01-01
11. CONTROLLING OFFICE NAME AND ADDRESS:
12. REPORT DATE: 7 May 1975
13. NUMBER OF PAGES: 30
14. MONITORING AGENCY NAME & ADDRESS (if different from Controlling Office):
15. SECURITY CLASS. (of this report): Unclassified
15a. DECLASSIFICATION/DOWNGRADING SCHEDULE:
16. DISTRIBUTION STATEMENT (of this Report): Approved for public release; distribution unlimited
17. DISTRIBUTION STATEMENT (of the abstract entered in Block 20, if different from Report):
18. SUPPLEMENTARY NOTES:
19. KEY WORDS (Continue on reverse side if necessary and identify by block number): Sphere, Hemisphere-Cylinder, Water Entry
20. ABSTRACT (Continue on reverse side if necessary and identify by block number):

An experimental investigation of the vertical water entry deceleration of a sphere and a hemisphere-cylinder is described. A common total drag is determined as a function of penetration distance. This result is compared to the result of previous investigators with good agreement occurring with the theory of M. Shiffman and D. C. Spencer and the experiments of C. R. Nisewanger. Possible errors introducted by extrapolation of this result to higher entry speeds are estimated.

DD FORM 1 JAN 73 1473 EDITION OF 1 NOV 65 IS OBSOLETE S/N 0102-014-6601

UNCLASSIFIED

SECURITY CLASSIFICATION OF THIS PAGE (When Data Entered)

391 596

NSWC/WOL/TR 75-49 7 May 1975

VERTICAL WATER ENTRY OF SPHERES

This report is a result of the continuing effort of the Naval Surface Weapons Center in the understanding of water-entry phenomena. The research reported herein was supported entirely by NAVSEA Code 03512 under task ORD-35B-001/UR109-01-01. The authors would like to acknowledge Dr. Thomas Peirce of NAVSEA for his advice and interest in this program.

V. C. D. Dawson
By direction

CONTENTS

ILLUSTRATIONS

TABLES

LIST OF SYMBOLS

A	cross-sectional area $A = \pi R^2$
B	buoyancy force
b	dimensionless depth $b = S/R$
C	speed of sound in the fluid
C_d	drag coefficient $C_d = \frac{2Fd}{\rho AU^2}$
F_d	drag force
g	gravitational constant
M	mass of the model
m	added mass
P	pressure
R	radius of the sphere
r	a radius taken in a plane parallel to the water surface
S	distance moved after water contact
s	distance
t	time
U	instantaneous model speed
W_b	wetting factor
θ	angle θ = arc sin R/R
ρ	mass density of the fluid

INTRODUCTION

The water entry of spherical shapes has been investigated for many years. Worthington and Cole reported on splashes caused by spheres impacting fluids in 1897 (Ref. (1)). The resistance that occurred during entry was measured by Watanabe before 1934 (Ref. (2)). Many other investigators have studied the phenomena both experimentally and theoretically. A force gage or an accelerometer was used as the basic transducer in tests reported by Blundell (Ref. (3)), Mason and Slichter (Ref. (4)), Richardson (Ref. (5)), Hobbs (Ref. (6)), Weible (Ref. (7)), and Mosteller (Ref. (8)). A pressure gage mounted flush to the spherical surface at several locations was added in the investigation of Nisewanger (Ref. (9)). Theoretical considerations included the expanding disk model employed by Plesset (Ref. (10)) and an expanding lens model corrected for free surface motion used by Shiffman and Spencer (Ref. (11)). Some of their experimental results are given in Figure 1. Inspection of these results showed a wide scatter in the predicted impact drag coefficient; therefore, it was decided to conduct a short experimental program to determine the vertical impact drag coefficient for spheres.

EXPERIMENTAL PROGRAM

A five-inch-diameter 1629-gram spherical model and a five-inch 1070 gram hemispherical-cylinder model were dropped vertically into water. The resulting deceleration was measured electronically. Impact speed was varied from 15 to 23 feet per second.

EXPERIMENTAL TECHNIQUE

The deceleration of models resulting from vertical water entry has been measured at NAVSURFWPNCEN for many years. A standard experimental setup has evolved for use in the Hydroballistics Facility and the related Pilot Tank. Results obtained using this method for cone, cusp, and ogive-shaped forebodies were reported in References (12) and (13). The model, containing a single-axially mounted crystal accelerometer, was dropped from a suitable height such that normal impact with the water surface resulted. A cable (trailing wire) connected the accelerometer within the model to electronic equipment located outside the test tank. The final output of the gage was displayed on a CR oscilloscope and photographically recorded. A light screen located near the water surface was interrupted by the model which triggered a strobe lamp unit. Three or four flashes equally spaced in time illuminated the model in the darkened tank. A plate camera with open shutter recorded the position and attitude of the model. Located in the light beam from the

strobe lamp was a photo-pickup that converted the light pulse into a voltage pulse that was also displayed on the CR oscilloscope. The arrangement of the equipment used in these tests is shown in Figure 2. The data resulting from this technique are contained in two photographs; one showing the model above the water surface at several points in time, the other showing the voltage output of the accelerometer and the time of each model image on a common time base. Figures 3 and 4 show samples of these data.

Two different models were used in this test series. A three-inch-diameter aluminum hemispherical head was fitted to a nylon cylindrical afterbody to form a model with relative mass of (2.42 gm/cm^3).

The second model was a five-inch-diameter duckpin bowling ball fitted with an accelerometer mount which resulted in a relative mass of (.795 gm/cm^3). Drawings of the models are presented as Figures 5 and 6.

The commercially available accelerometers mounted in the models were made from quartz crystals and included internal electronics that provided low output impedance. A gage coupler attached to the fixed end of the trailing wire provided power to the gage and produced the input to the other electronics. With such a gage, insignificant errors resulted from the flexure or acceleration of the trailing wire. Gage constants were obtained by comparing the outputs of the test gage with a standard gage to which it had been piggybacked in a simple impact fixture. The remaining electronics were calibrated several times during the tests by introducing a known voltage in place of the gage coupler.

DATA REDUCTION AND RESULTS

The "a priori" assumptions that were made in the data reduction included:

1. The hydrodynamic forces depended only upon size, geometry, actual velocity squared and distance below the water surface.

2. Buoyancy force was calculated from the original water surface.

3. Friction drag was negligibly small.

The preliminary data reduction was done manually and involved changing the photographic records to digital form. Water impact velocity was obtained from the plate camera film as follows: the distance the model advanced between strobe flashes was computed using the diameter of the model as the reference dimension. The time between flashes had been measured by an electronic counter during the test. Average air velocity was computed by dividing the change in position of the model by the change in time in which this occurred. The impact velocity was obtained by adding the change in velocity due to gravity between the time of the average air velocity and the time of impact. The readings of the oscilloscope records were made using a toolmaker's microscope in the following order: the distance of a vertical grid unit was measured to determine the scale factor; next, a point on the accelerometer trace just before impact was read and then a series of points along the trace was read.

The sphere model was dropped without benefit of a guide tube which resulted in some rotation before impact. Thus, the axis of the accelerometer was not vertical during entry and measured only a component of the vertical deceleration. In order to compensate for this error, an effective gage constant was computed for each test by dividing the standard gage constant by the cosine of the true angle between the vertical and the axis of the accelerometer. This angle was obtained from the plate camera pictures.

The numbers obtained from the pictures along with information such as model diameter, weight, effective gage constant and scope gain were entered into a time-shared digital computer which calculated the drag coefficient function as follows:

1. The acceleration time data were converted to English engineering units for computations such that zero volts and 32.2 feet/second acceleration occurred just before impact.

2. An RC leakage correction was applied to the acceleration data.

3. The velocity and distance after impact were determined at each data point by trapezoidal integrations.

4. The drag coefficient was computed at each data point using

$$-\frac{dU}{dt}(M + m) - B + Mg = \frac{1}{2}\rho C_d A U^2 \qquad (1)$$

where the added mass (m) was assumed to be equal to zero.

5. The value of added mass was computed at each data point by trapezoidal integration using

$$\frac{dm}{ds} = \frac{\rho}{2} AC_d \qquad (2)$$

6. Steps four and five were then repeated three times using the latest value of added mass or drag coefficient. The results of the data reduction are shown on Figure (7).

DISCUSSION

A low pass electronic filter was used during this test to attenuate spurious signals. The need to use such a filter was evident from the data traces (Fig. (4)) which showed a measururable amount of ringing at 3.5 kilohertz after attenuation of about eight db (60 percent). The magnitude of the errors caused by the filter depended upon the separation of the highest frequency present in the data from the filter cutoff frequency. The minimum separation ratio was estimated as .3. At this ratio the information supplied by the filter manufacturer showed no change in amplitude and a phase lag of 35 degrees for the highest frequency present in the data. Hence, the trace may have been compacted by as much as ten percent between water contact and the point of maximum drag coefficient.

The entry velocities obtained during these tests and those reported in the references were much slower than those of most applications. Engineering usefulness of such data depends upon the accuracy with which the test results can be extrapolated to application conditions. Extensive experimental investigations on the vertical entry of various cones did not show a significant change in the drag coefficient function when base diameters varied from 1.5 inches to 1.5 feet or when entry velocities changed from ten to 200 feet per second (Refs. (12) and (14)).

The water-entry phenomena of spheres differ in at least one aspect from the entry of cones. A shock phase always occurs during sphere entry and only at very high velocities for cones.

When a sphere impacts the water, at any speed, there exists a region where the circle of first contact expands at a radial rate greater than the speed of sound in water. The pressures acting within this region were estimated by consideration of the following simple model.

a. the nose was replaced by surface sources,
b. the water was considered to be compressible,
c. the water was not allowed to flow radially.

In this case a shock was generated at the contact circle that curved inward and away from the nose as it became weaker as shown on Figure (8). The pressures at least near the contact ring were estimated to be given by

$$P = \rho C U \tag{3}$$

The shock occurred only at the body when the rate of expansion of the contact surface exceeded the speed of sound in water. The angle at which the shock disappeared was called the critical angle and was computed from equation (4). For small θ, the corresponding radius was calculated using equation (5)

$$\theta_{crit} = \text{arc tan } U/C \tag{4}$$

$$r_{crit} \approx RU/C \tag{5}$$

Then the maximum contribution to the drag coefficient of the shock phase was calculated based upon the additional assumption that the pressure inside the shock was constant

$$F_d = \rho C U \pi (r_{crit})^2 = 1/2 \rho C_d \pi R^2 U^2$$

$$C_d = \frac{2C}{U} \left(\frac{r_{crit}}{R}\right)^2 \approx 2 \frac{U}{C} \tag{6}$$

The distance moved after first contact until r_{crit} occurred was computed from

$$S_{crit} = R \left(1 - \cos \frac{U}{C}\right) \tag{7}$$

or

$$S_{crit} \approx \frac{R}{2} \left(\frac{U}{C}\right)^2 \tag{8}$$

The drag coefficient from water contact until loss of the shock was calculated as equation (9)

$$F_d = \rho C U \pi r^2 = 1/2 \rho C_d \pi R^2 U^2$$

$$C_d = \frac{2Cr^2}{UR^2} = \frac{2C\ (R \sin \theta)^2}{UR^2} = \frac{2C \sin^2 \theta}{U} \tag{9}$$

The dimensionless depth of the model was calculated as

$$\frac{S}{R} = (1 - \cos \theta) \tag{10}$$

and the slope of the line from the origin to the drag coefficient function for a given θ was given by

$$\frac{C_d}{\left(\frac{S}{R}\right)} = \frac{2C \sin^2 \theta}{U(1 - \cos \theta)} = \frac{2C}{U}(1 + \cos \theta) \qquad (11)$$

For small angles of θ, equation (11) was approximated by

$$\frac{C_d}{\left(\frac{S}{R}\right)} \approx \frac{4C}{U} \qquad (12)$$

Therefore, the drag coefficient curve should be a straight line from the origin to a depth of $\frac{S}{R} = (1 - \cos U/C)$ and then bend away from the vertical.

Predicted shock phase values were computed for a typical experimental entry of 25 feet per second with a five-inch-diameter sphere and at a possible application entry velocity of 150 feet per second. These predicted values are compared with experimental values in Table 1 to show the relative importance of the shock phase.

Table 1

Comparison of Maximum Characteristic Parameters for the Shock Phase with Comparable Experimental Values

	U = 25 ft/sec	U = 150 ft/sec	Experimental
θ (degrees)	.3 (crit)	1.8 (crit)	27 ($C_{d_{max}}$)
r (inches)	.013 (crit)	.078 (crit)	1.14 ($C_{d_{max}}$)
C_d	.01 (crit)	.0625 (crit)	1.05 ($C_{d_{max}}$)
$\frac{S}{R}$	.0001 (crit)	.00049 (crit)	.11 ($C_{d_{max}}$)
$C_{d_{slope}}$ at (0,0)	768	128	59

The conclusion obtained from this analysis was that the shock phase produced high pressures over a small area of the nose for very short periods of time and would not significantly alter the drag coefficient function at entry velocities below 300 feet per second. Results from a more accurate model would probably show that the pressure acts upon an area larger than that determined by the original water surface.

Experiments have shown that the pressure wave moves about 50 percent faster than the original water surface both for the vertical entry of blunt cones and the oblique entry of disk cylinders (Ref. (14)). Such an effect would increase the predicted values given in Table 1 by 50 percent except C_d(crit) which would increase by 125 percent. These changes are not enough to change the above conclusions.

In 1934 S. Watanabe published the results of his experiments that investigated the water-entry resistance of a sphere (Ref. (2)). In these tests he dropped a model with a spherical segment head from heights of 20, 30, 40 and 50 centimeters into a water tank. The geometric dimensions of the head were: radius of curvature - 15 centimenters, diameter of head - ten centimeters, height of spherical surface - .84 centimeters, and total height of head - 1.6 centimeters as shown on Figure (9). Between the head and the main mass of the model were located two quartz crystals that formed a force gage. He recorded the gage output on a cathode-ray oscillograph. This experimental technique had been developed over several years during his study of the water impact of cones, wedges and disks. However, his results gave a maximum drag coefficient of about .45 at a dimensionless depth of .02. The current tests gave corresponding values of 1.05 and 0.11. The dimensionless height of the spherical surface was about half of the distance a sphere moves from water contact until the maximum drag coefficient occurs. Hence, it was impossible for Watanabe to measure the maximum drag coefficient of a sphere using his spherical segment model.

Then, the shape tested by Watanabe was considered to be the spherical segment and the accuracy of his results estimated from existing cone data (Refs. (12) and (14)). It was expected that the results for spherical segmentswould be bounded by results for the two cones that bounded the spherical surface. The two cones selected were a disk, (180-degree cone) tangent to the tip of the segment, and a 140-degree cone, tangent to the base of the segment. The maximum drag coefficient and associated depth and added mass were chosen as representation parameters. For the spherical segment, the added mass was calculated from Watanabe's data using two iterations of equations (1) and (2) and the drag coefficient was based on the actual ten-centimeter diameter of the model. The numerical results were assembled as Table 2.

Table 2

Comparison of Results for Sphere Segment with Bounding Cones

	Disk	Sphere Seg.	140° Cone
$C_{d(max)}$	>5.55	4.30	5.55
S/R (at $C_{d(max)}$)	.61	.41	.72
Added mass (at $C_{d(max)}$) grams/(Dia. in cm)^3)	.123	.050	.097

The comparison of results showed that in all cases the values for the spherical segment fell outside the values for the two cones that geometrically bound the segment. Therefore, the accuracy of Watanabe's data was not shown. Future tests of spherical segments should be considered.

In 1954 C. R. Nisewanger measured the pressure field and the deceleration that acted on a hemisphere during water impact at 23.5 feet/second (Ref. (9)). The model had a 12-inch-diameter with a one-inch wall. One pressure gage and one accelerometer were mounted within the model during the test. Different locations of the pressure gageswere obtained by changing models and by rocking the model in the test fixture. Thus, many tests were required to obtain the pressure field. This important work was terminated prematurely and not reported until 1961 which is perhaps why it has not received wide recognition.

One objection might have been that Nisewanger neglected to list the effective mass of the impact model; hence, it was impossible to correct the results to infinite mass conditions. This objection was investigated as follows: it was observed that Nisewanger's drag coefficient function had the shape associated with the entry of a heavy sphere. The minimum effective impact mass of Nisewanger's model was estimated to be 40,400 grams (relative mass 1.42 gms/cm^3) from information in Reference (9). The errors in maximum drag coefficients associated with a sphere of minimum mass of 1.42 gms/cm^3 were estimated to be smaller than 15 percent (the added mass associated with the maximum drag coefficient was taken as .067 gms/cm^3). No corrections were made to the data presented by Nisewanger because the actual mass of his model may have been several times larger than the calculated minimum.

The results of the current tests were compared with the experimental drag coefficient function of C. Nisewanger, (Ref. (9)) and the theoretical prediction of M. Shiffman and D. C. Spencer on Figure (10). The three functions agreed to within a range of ten percent from water contact until the maximum drag coefficient occurred. At depths greater than S/R = .6, the theoretical curve fell below the experimental curves because the theory used did not account for steady drag effects.

On Figure (11) were plotted the maximum pressure coefficients as a function of gage location as reported by Nisewanger (Ref. (9)). Also shown was the maximum pressure coefficient of a 140-degree total angle cone (Ref. (14)). Agreement to within five percent resulted between the maximum pressures measured on sphere and the cone.

The rate at which the pressure force moved across the sphere was measured by C. Nisewanger. A least square fit to the data resulted in the wetting factor (W_b) being given by:

$$W_b = 1.736 - 0.586 \sqrt{b}$$

where

$$b = \frac{S}{R}$$

The initial wetting factor ($W_b = 1.736$) was compared to the wetting factor for the vertical entry of disk cylinders. Based upon accelerometer data, the wetting factor for disk cylinders was shown to be $W_b = 1.626$ for all entry angles. It was observed that the pressure front moves at least as fast as the acceleration which may have caused the seven percent difference in wetting factor.

CONCLUSIONS AND RECOMMENDATIONS

1. The average curve shown on Figure (7) represents the water-entry drag coefficient of a sphere at moderate speeds to within ten percent.

2. The results of S. Watanabe do not represent the water entry of a sphere.

3. The pressure distributions of C. Nisewanger represent the best available data.

4. Additional studies should include the shock phase of sphere entry and an investigation of the water entry of spherical segments.

REFERENCES

1. A. M. Worthington and R. S. Cole, "Impact with a Liquid Surface, Studied by the Aid of Instantaneous Photography", Phil. Trans. Roy Soc. 189A, 137-148 (1897)

2. S. Watanabe, "Resistance of Impact on Water Surface, Part V - Sphere", Sc. Pap. Inst. P. C. Res. 23, 202-208 (1934)

3. R. W. Blundell, "Force Measurements on a Hemisphere when Dropped into Water", Marine Aircraft Exptl Est., Flixtowe (Min. of Sup.) Rept. F/Res/106 (1937)

4. Office of Scientific Research and Development, "Water Entry and Underwater Ballistics of Projectiles", OSRD Rept. 2551, CIT (1946)

5. E. G. Richardson, "The Impact of a Solid on a Liquid Surface", Proc. Phys. Soc. (London) 61, 352-367 (1948)

6. E. V. Hobbs, "Experimental Determination of Virtual Water Mass from Measurement of Forces Developed during Entry of a Sphere into Water", NBS Rept. 6.4/196, Project No. 3518 (1950)

7. A Weible, "The Penetration Resistance of Bodies with Various Head Forms at Perpendicular Impact on Water", Naval Res. Lab. transl. 286 (1952)

8. G. G. Mosteller, "Axial Deceleration at Oblique Water Entry of Two-Inch-Diameter Models with Hemisphere and Disk-Cylinder Noses", NOTS NAVORD Rept. 5424 (1957)

9. C. R. Nisewanger, "Experimental Determination of Pressure Distribution on a Sphere During Water Entry", NAVWEPS Rept. 7808 (1961)

10. M. S. Plesset, "Investigation of the Impact Force on Torpedoes Entering Water", Douglas Aircraft Co., Rept. SM 3937 (1942)

11. M. Shiffman and D. C. Spencer, "The Force of Impact on a Sphere Striking a Water Surface" (Second Approximation) NDRC AMP Rept. 42.2R (1945)

12. J. Baldwin, "Vertical Water Entry of Cones", NOLTR 71-25 (1971)

13. J. Baldwin, "Vertical Water Entry of Some Ogives, Cones, and Cusps", NSWC/WOL/TR 75-20 (1975)

14. J. Baldwin, "An Experimental Investigation of Water Entry", Ph.D., University of Maryland (1972)

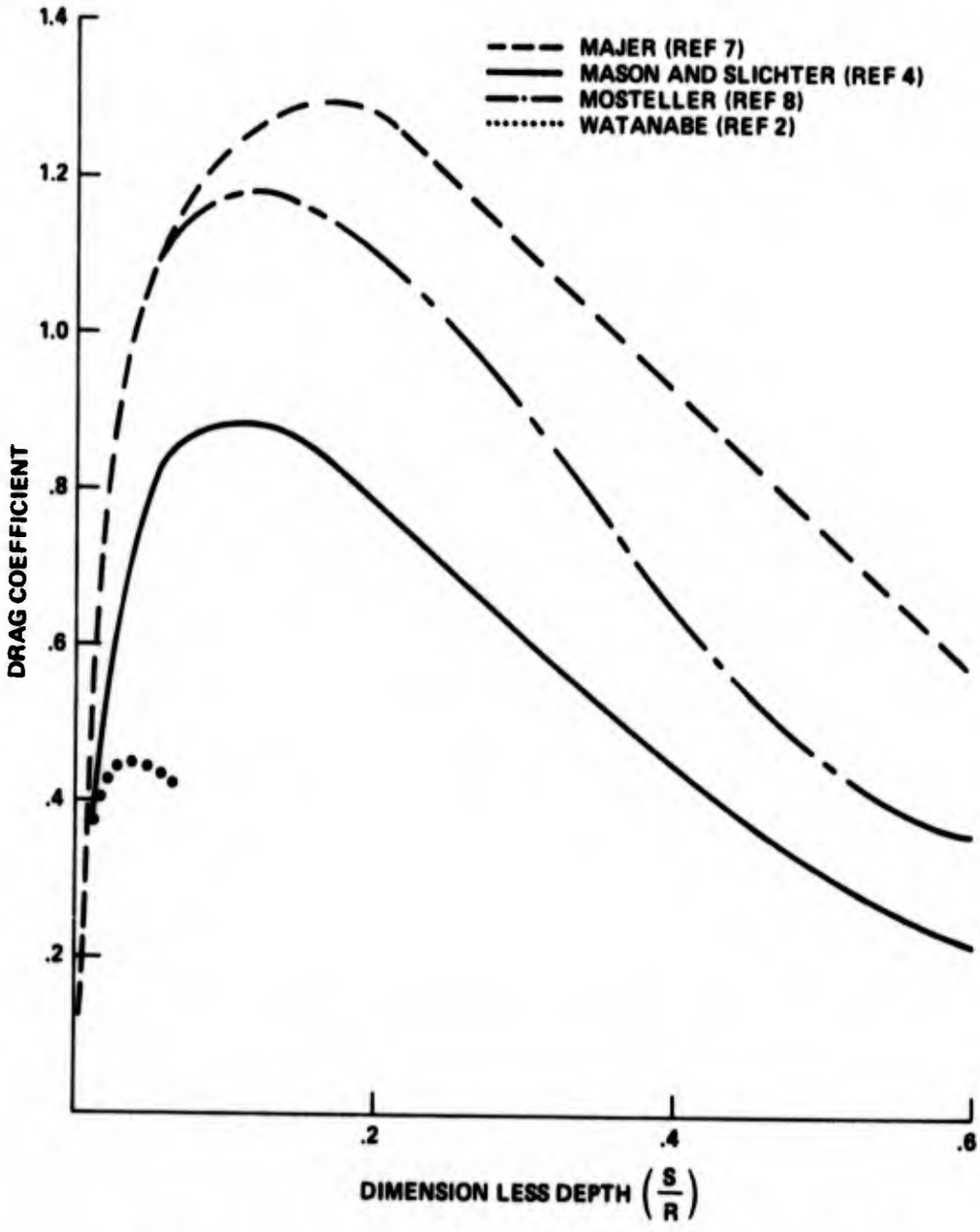

FIG. 1 SELECTED PAST EXPERIMENTAL WATER IMPACT DRAG COEFFICIENT FOR SPHERES

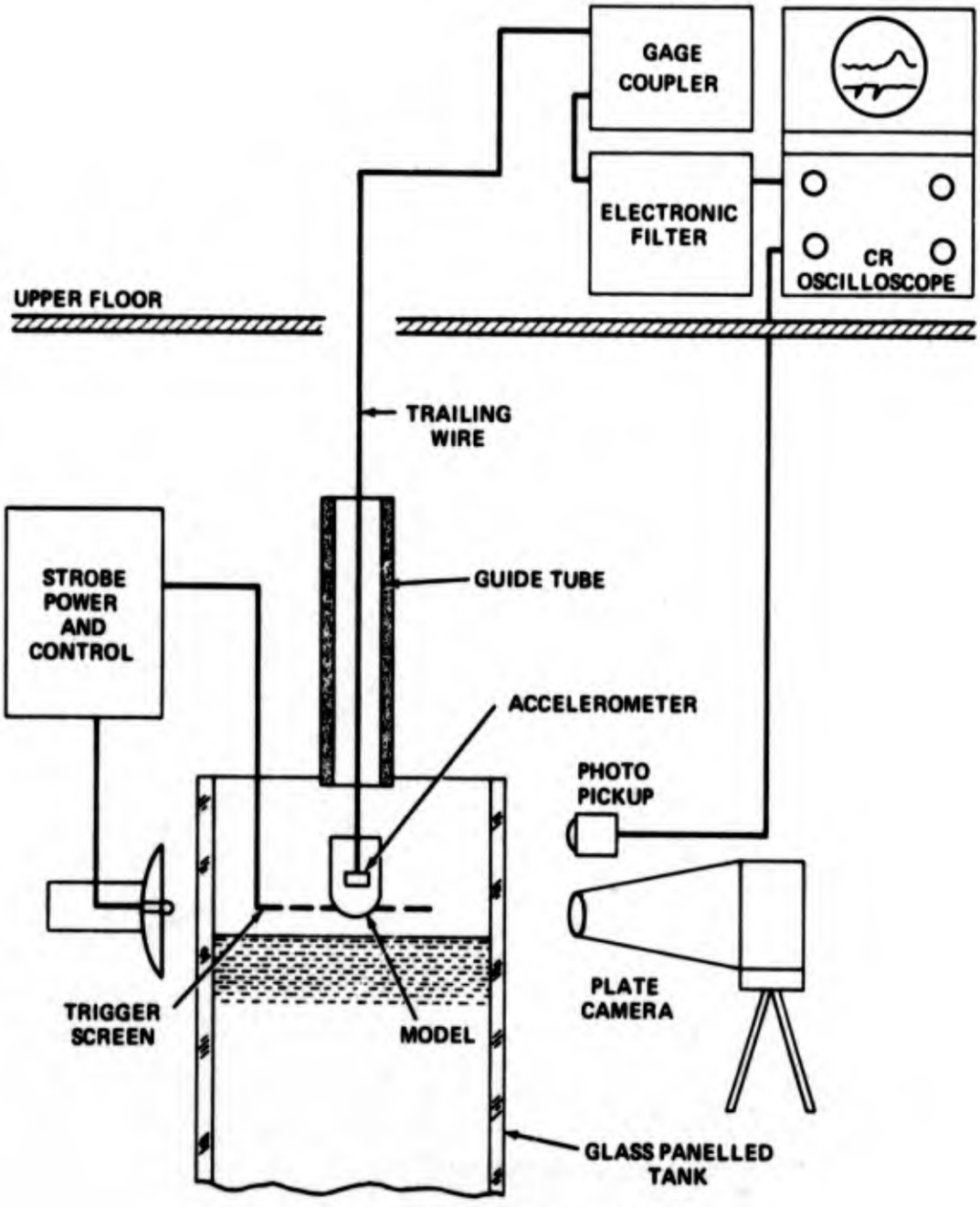

FIG. 2 TEST EQUIPMENT SCHEMATIC

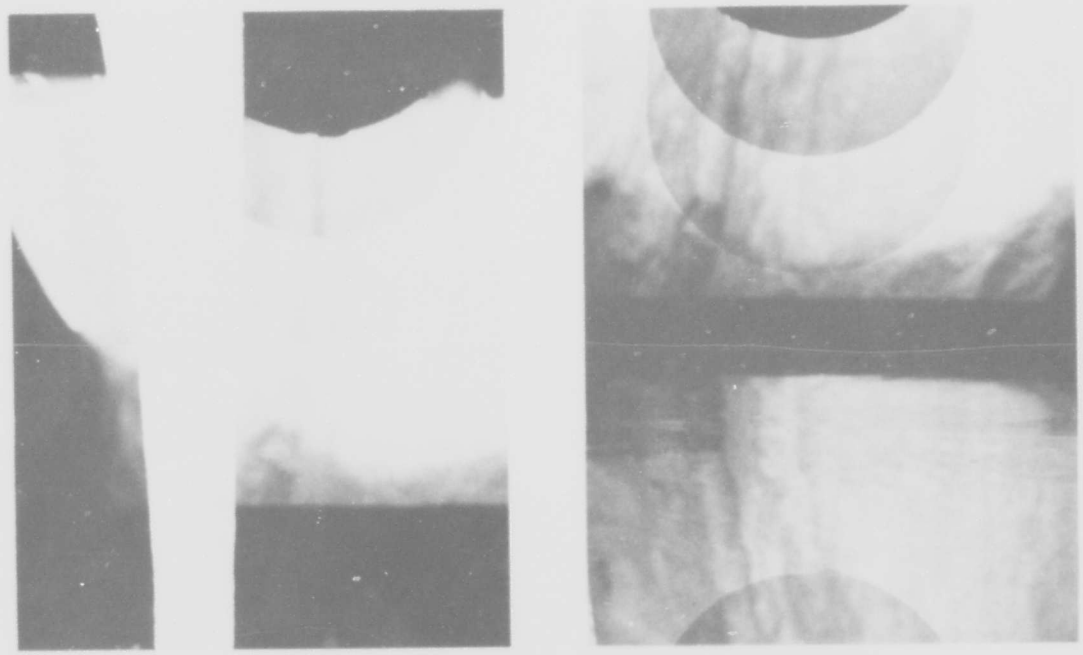

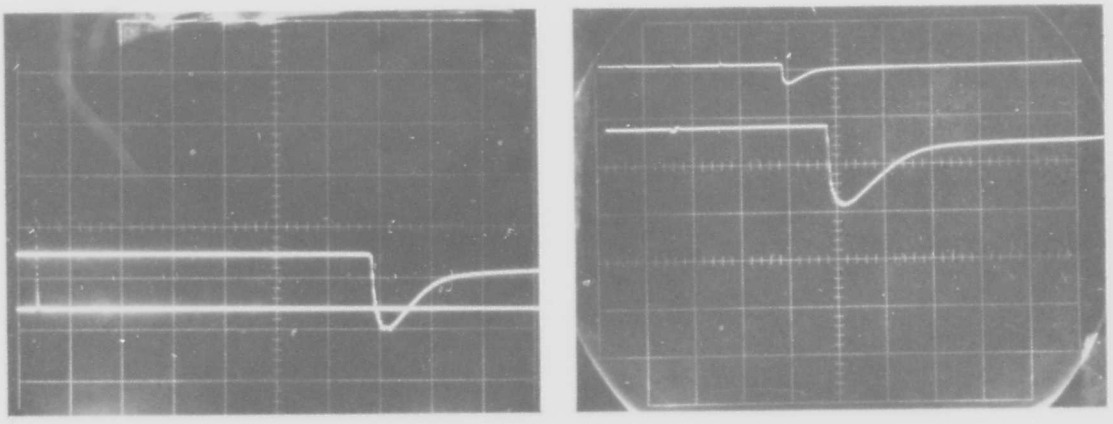

TEST NO. 802

2 MSEC/CM
0.1 VOLT/CM

7KC LOW PASS FILTER
2802 FT/SEC^2/VOLT

TEST NO. 805

5 MSEC/CM
0.2 VOLT/CM } UPPER TRACE

2 MSEC/CM
0.05 VOLT/CM } LOWER TRACE

5KC LOW PASS FILTER
2802 FT/SEC^2/VOLT

FIG. 3 SAMPLES OF TEST DATA (HEMISPHERE CYLINDER)

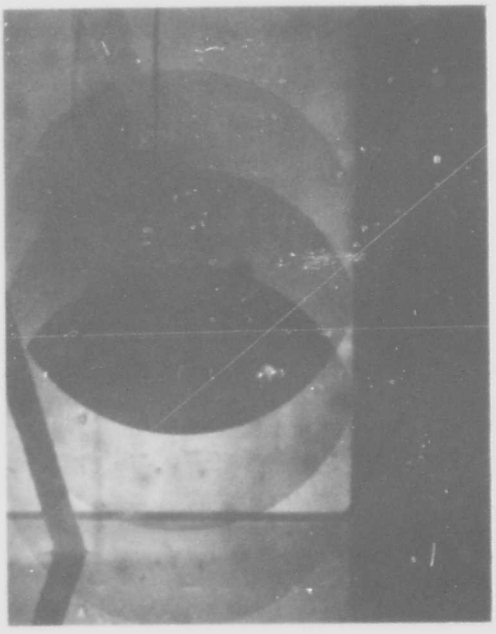

DROP NO. 6 3 NOV 71 Hv Mc 5.004 msec/p

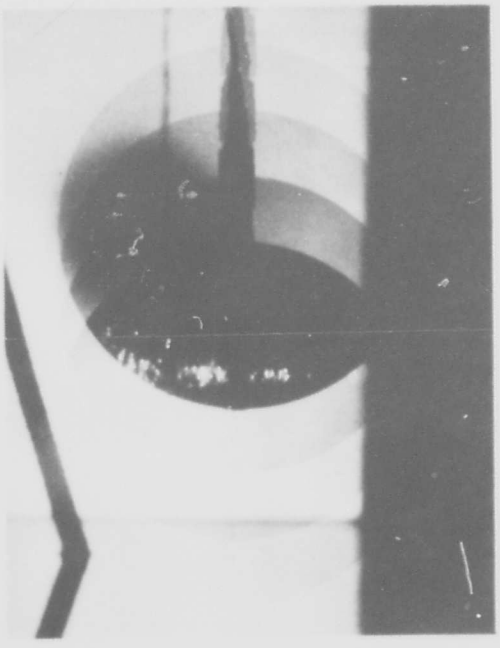

DROP NO. 8 3 NOV 71 HvHc 5.022 msec/p 4 FLASHES

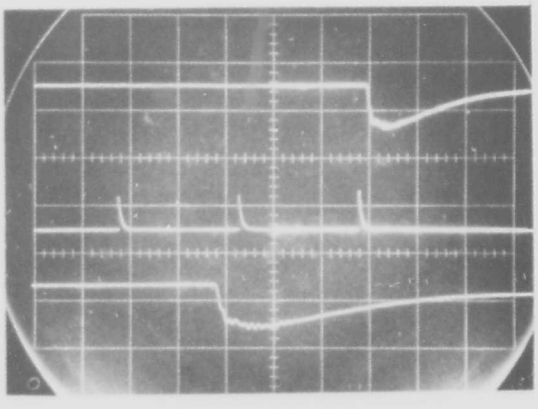

TEST NO. 226

2 MSEC/CM
0.02 VOLT/CM

1 MSEC/CM
0.02 VOLT/CM

2.5KC LOW PASS FILTER
30,925 FT/SEC^2/VOLT

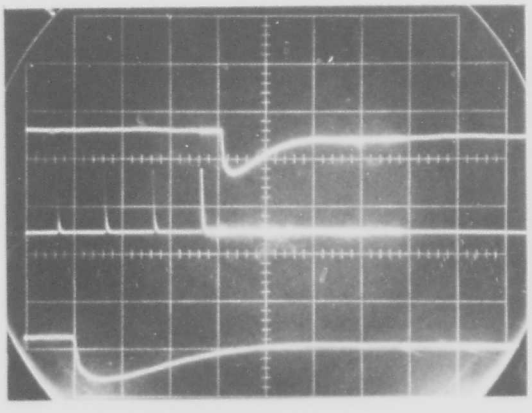

TEST NO. 228

5 MSEC/CM
0.01 VOLT/CM } UPPER TRACE

2 MSEC/CM
0.01 VOLT/CM } LOWER TRACE

2.5KC LOW PASS FILTER
29,324 FT/SEC^2/VOLT

FIG. 4 SAMPLES OF TEST DATA (SPHERE)

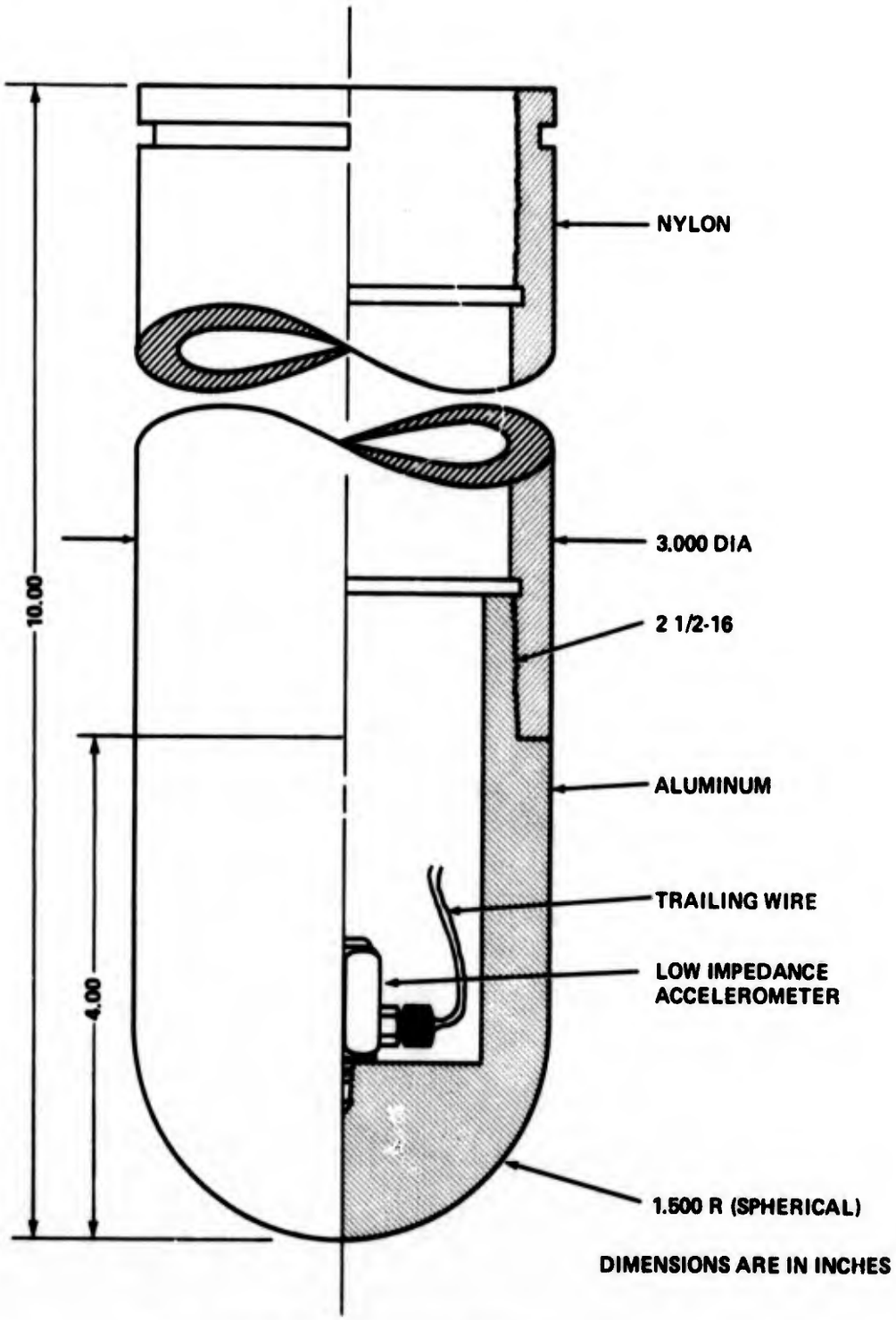

FIG. 5 HEMISPHERE-CYLINDER MODEL

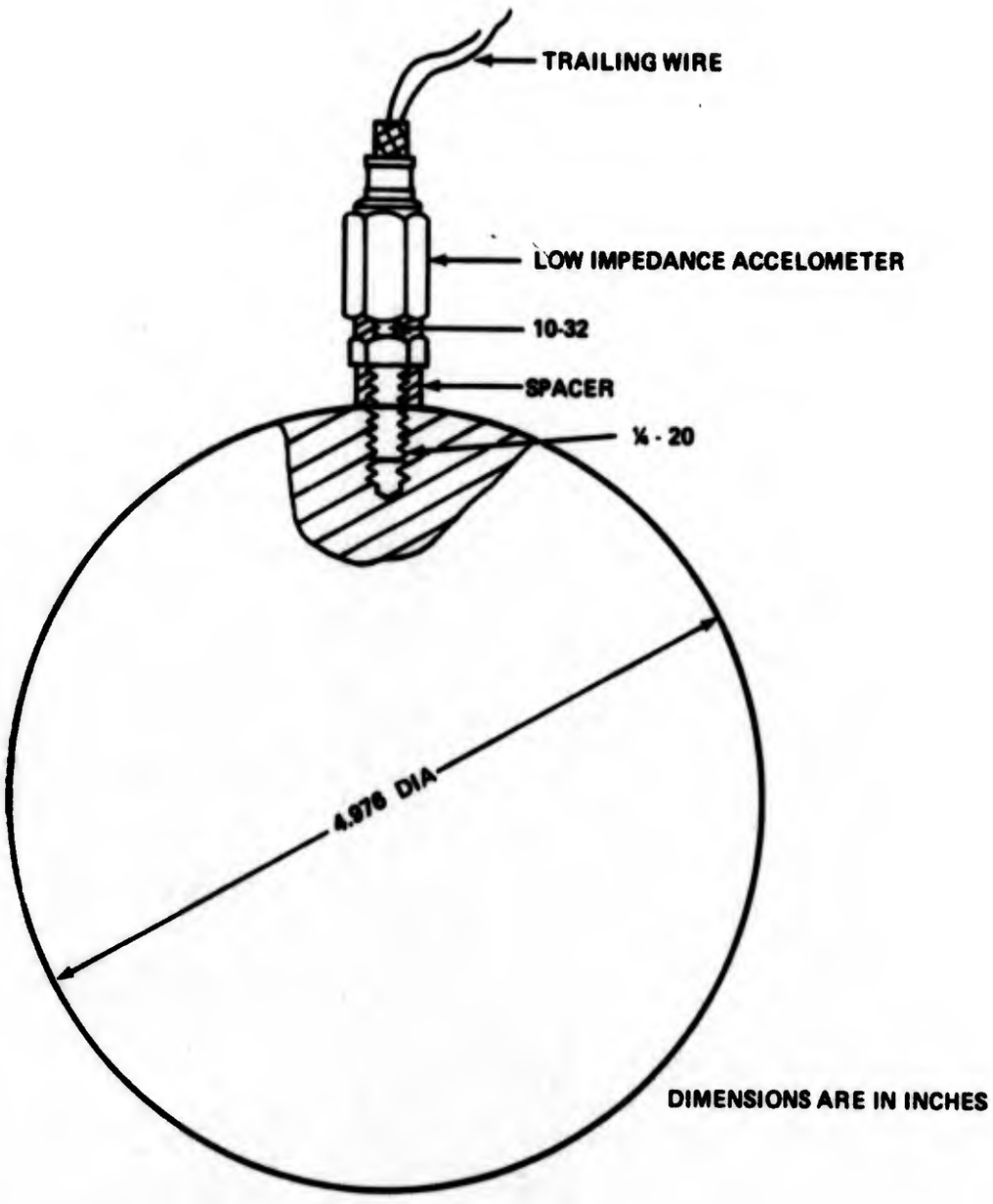

FIG. 6 SPHERE MODEL

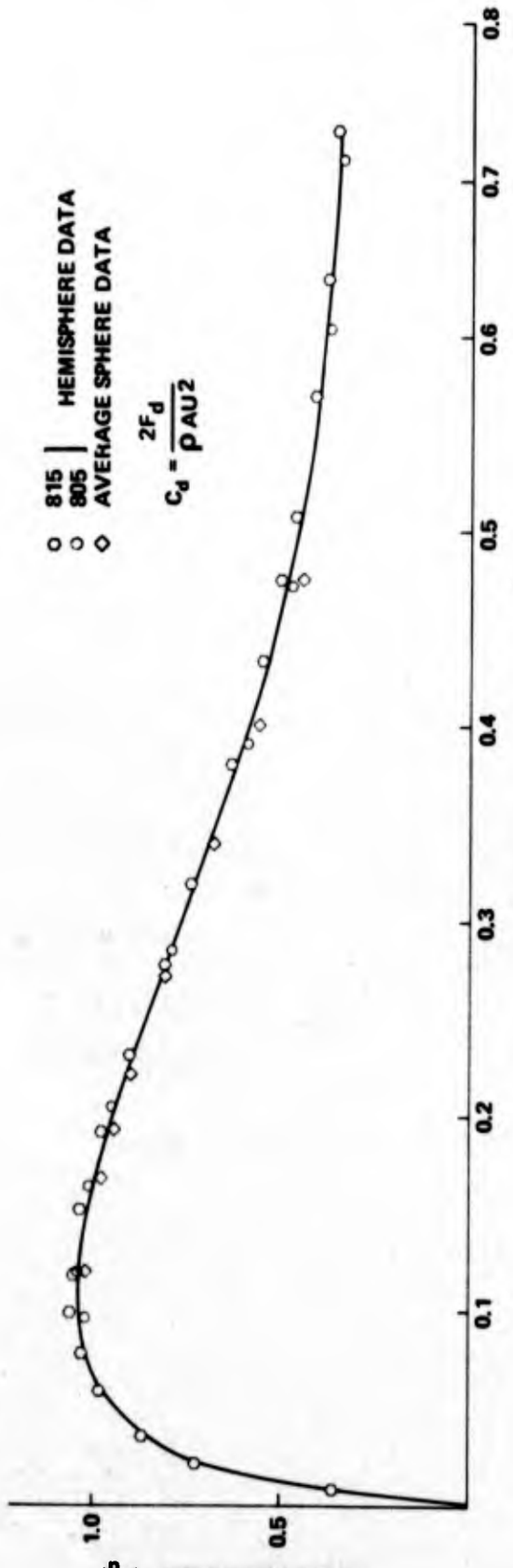

FIGURE 7 VERTICAL IMPACT DRAG COEFFICIENT FOR SPHERES

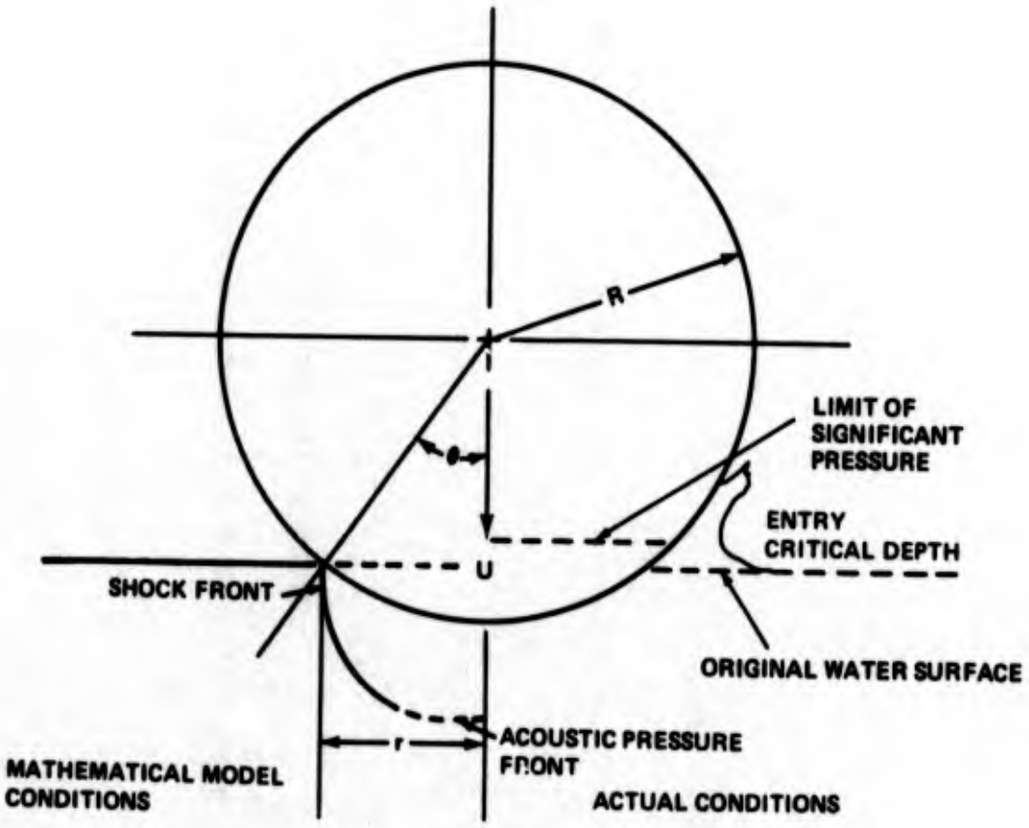

FIG. 8 WATER ENTRY GEOMETRY FOR A SPHERE

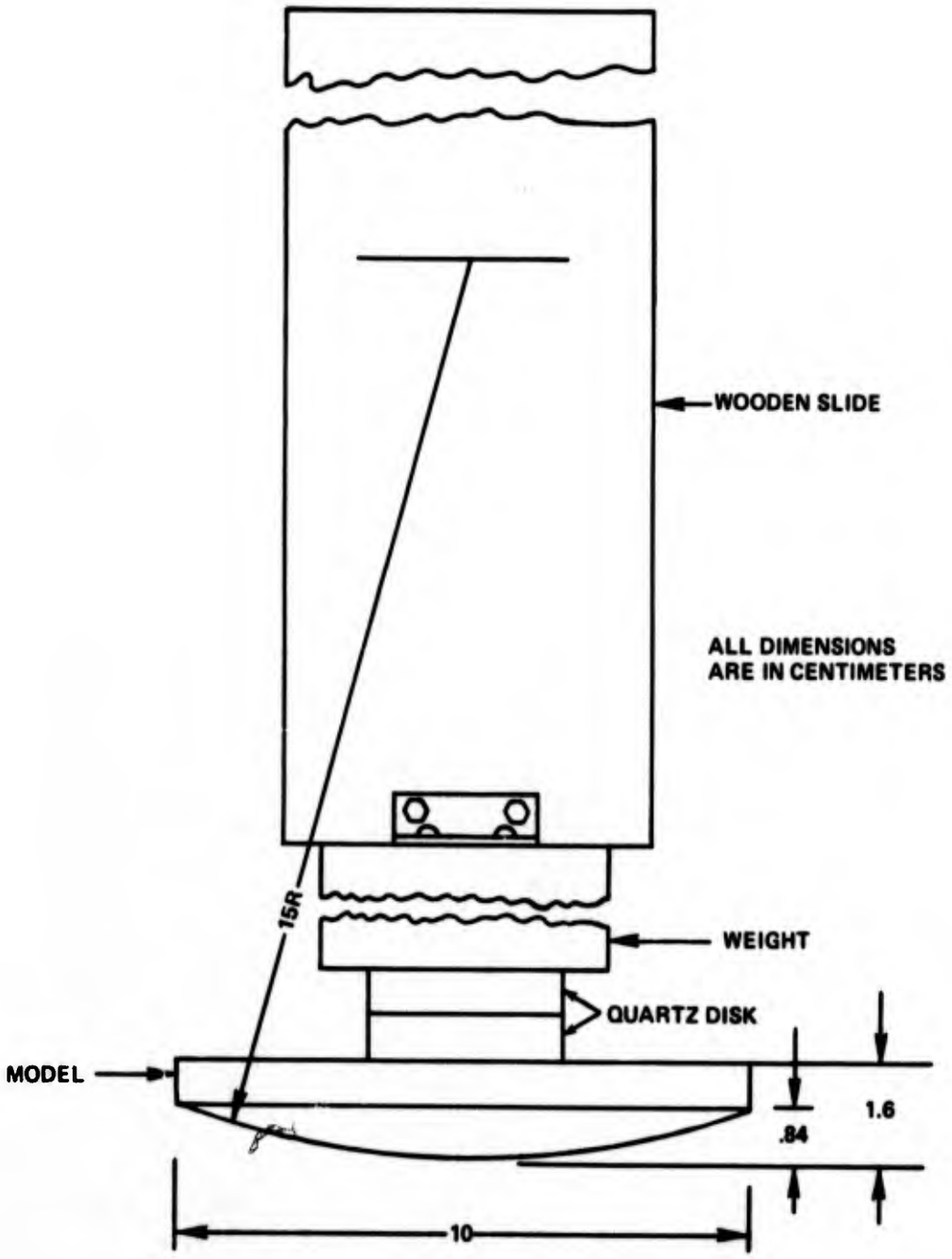

FIG. 9 WATANABE'S SPHERE SPHERICAL SEGMENT FALLING BODY

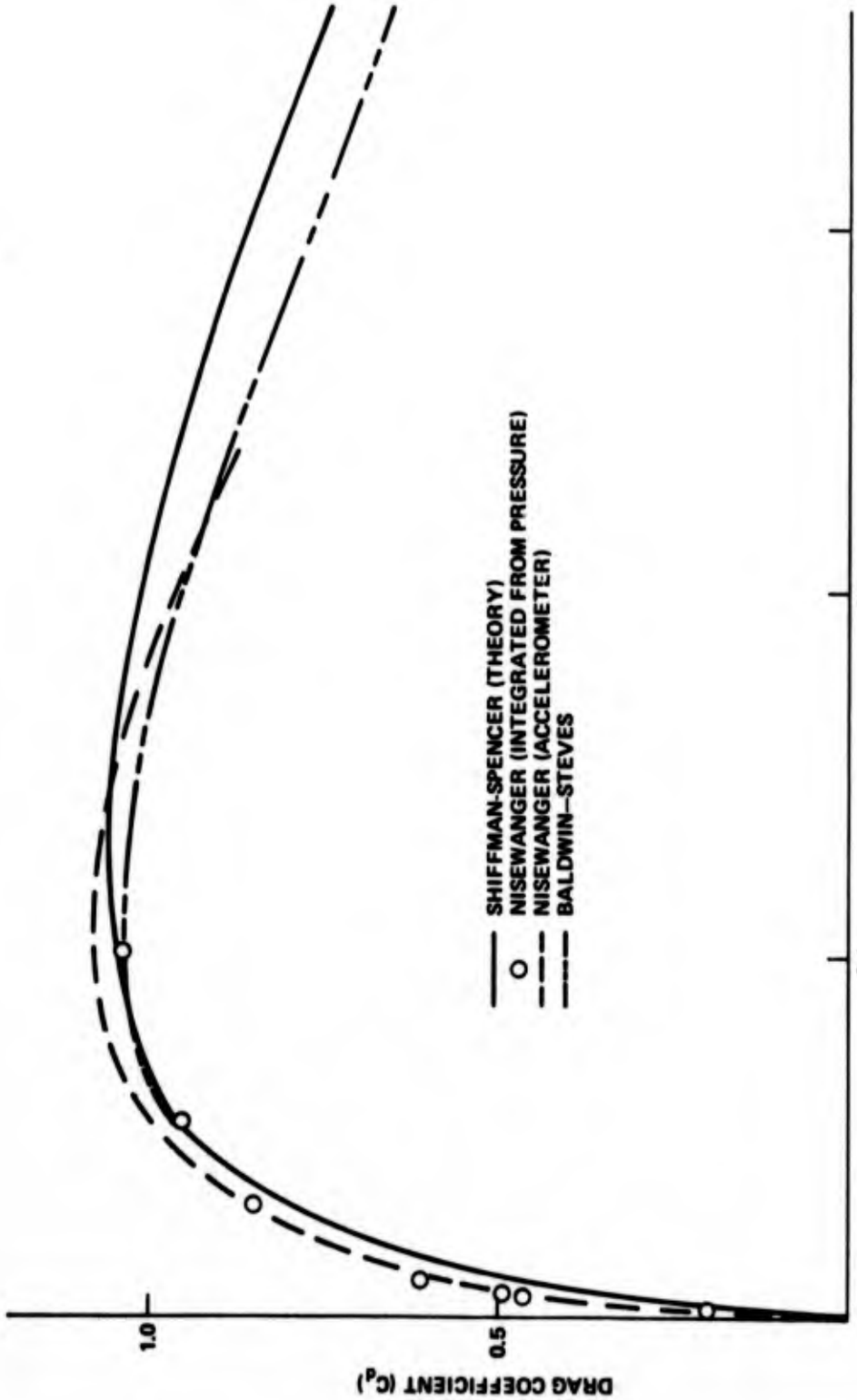

FIG. 10 COMPARISON OF THEORETICAL AND EXPERIMENTAL VERTICAL IMPACT DRAG COEFFICIENTS FOR SPHERES

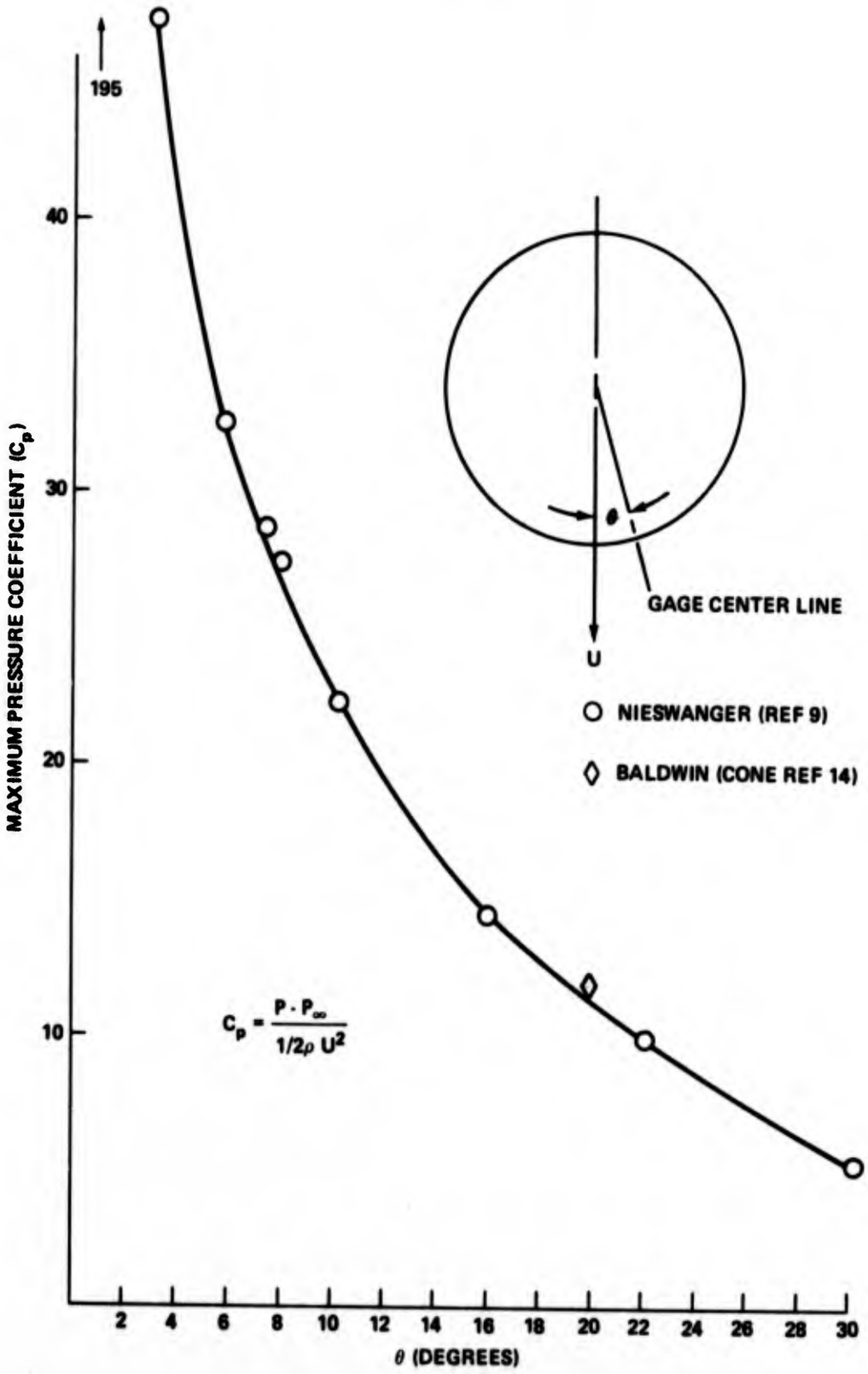

FIG. 11 MAXIMUM PRESSURE COEFFICIENT AS A FUNCTION OF GAGE LOCATION

DISTRIBUTION

Copies

Commander
Naval Air Systems Command
Washington, D. C. 20362
Attn: AIR-530133A
AIR-53712A
AIR-350D
AIR-350
AIR-350B
AIR-030

Commander
Naval Sea Systems Command
Department of the Navy
Washington, D. C. 20362
Attn: SEA- 09G32
SEA-03 B
SEA-0351
SEA-0372
SEA-054
SEA-05121
PMS-0647

Office of Naval Research
Department of the Navy
Arlington, Virginia 22217
Attn: ONR-438
ONR-439
ONR-463

Director
Defense Research and Engineering
The Pentagon
Washington, D. C. 20301

Defense Documentation Center
Cameron Station
Alexandria, Virginia 21314 12

Director of Research
National Aeronautics and Space Administration
600 Independence Avenue Southwest
Washington, D. C. 20546

NASA Scientific and Technical Information Facility
Post Office Box 33
College Park, Maryland 20740 2

Copies

Superintendent
U. S. Naval Postgraduate School
Monterey, California 93940
Attn: Library

Commanding Officer
U. S. Naval Air Development Center
Warminister, Pennsylvania 18974
Attn: NADC Library

Director
U. S. Naval Research Laboratory
Washington, D. C. 20390
Attn: Library 2

Commanding Officer
Naval Ship Research and Development Center
Bethesda, Maryland 20084
Attn: Code 154
Code 1541
Code 1556
Code 5613

Commander
Naval Undersea Center
San Diego, California 92132
Attn: Dr. A. Fabula
Dr. J. Hoyt

Commanding Officer
Naval Underwater Systems Center
Newport, Rhode Island 02840
Attn: J. F. Brady
W. A. McNally
R. H. Nadolink

Commander
Naval Weapons Center
China Lake, California 93555
Attn: Library 2

Harry Diamond Laboratories
Washington, D. C. 20438
Attn: Harry Davis
Library

U. S. Army Ballistic Research Laboratories
Aberdeen Proving Ground, Maryland 21105
Attn: Library

Copies

National Aeronautics and Space Administration
George C. Marshall Space Flight Center
Huntsville, Alabama 35812
Attn: Library

National Aeronautics and Space Administration
Langley Research Center
Langley Station
Hampton, Virginia 23365
Attn: Library

National Aeronautics and Space Administration
Lewis Research Center
21000 Brookpark Road
Cleveland, Ohio 44135
Attn: Library

Director
Alden Research Laboratories
Worcester Polytechnic Institute
Holden, Massachusetts 01520 2

Applied Physics Laboratory
The Johns Hopkins University
8621 Georgia Avenue
Silver Spring, Maryland 20910
Attn: Document Librarian 2

Applied Research Laboratory
The Pennsylvania State University
Post Office Box 30
State College, Pennsylvania 16801
Attn: Dr. Blaine R. Parkin
Dr. J. W. Holl

AVCO Everett Research Laboratory
2385 Revere Beach Parkway
Everett, Massachusetts 02149
Attn: Library

Battelle Memorial Institute
505 King Avenue
Columbus, Ohio 43201
Attn: Library

The Boeing Company Aerospace Library
Post Office Box 3999
Seattle, Washington 98124

Copies

Garfield Thomas Water Tunnel Library
The Pennsylvania State University
Institute for Science and Engineering
Applied Research Laboratory
Post Office Box 10
State College, Pennsylvania 16801

General Electric Company
Post Office Box 8555
Philadelphia, Pennsylvania 19101
Attn: MSD Library

Hydronautics, Incorporated
Pindell School Road
Laurel, Maryland 20810
Attn: Mr. Philip Eisenburg 2

Iowa Institute of Hydraulic Research
State University of Iowa
Iowa City, Iowa 52240
Attn: Dr. J. F. Kennedy 2

Jet Propulsion Laboratory
4800 Oak Grove Drive
Pasadena, California 91103
Attn: Library

Lockheed Missile and Space Company
Missile System Division
Post Office Box 504
Sunnyvale, California 94086
Attn: Mr. Robert Waid 2

Los Alamos Scientific Laboratory
Post Office Box 1663
Los Alamos, New Mexico 87544
Attn: Report Library

Sandia Laboratories
Albuquerque, New Mexico
Attn: Mr. A. Stephenson
Library

Director
Southwest Research Institute
Department of Mechanical Sciences
San Antonio, Texas 78206
Attn: Library